Quantitative measurement of blood velocity in zebrafish with optical vector field tomography

Luca Fieramonti[1], *Efrem A. Foglia*[2], *Stefano Malavasi*[3], *Cosimo D'Andrea*[1], *Gianluca Valentini*[1], *Franco Cotelli*[2], *and Andrea Bassi*[*,1]

[1] Politecnico di Milano, Dipartimento di Fisica, piazza Leonardo da Vinci 32, Milano, Italy
[2] Università degli Studi di Milano, Dipartimento di Bioscienze, via Celoria 26, Milano, Italy
[3] Politecnico di Milano, Dipartimento di Ingegneria Civile e Ambientale, piazza Leonardo da Vinci 32, Milano, Italy

Received 10 October 2013, revised 15 November 2013, accepted 25 November 2013
Published online 12 December 2013

1. Introduction

In vertebrates, blood flow parameters play a key role in angiogenesis and vasculogenesis [1, 2]. The interplay between functional parameters and gene expression is increasingly studied in developmental biology and genetics. The small and transparent zebrafish (*Danio rerio*) embryo provides an ideal animal model to achieve high-resolution imaging of superficial and deeply localized vessels. Zebrafish vascular imaging has progressed tremendously in recent years [3–5], however quantitative methods able to provide blood flow parameters are still highly desirable. Correlative techniques, such as Fluorescence Correlation Spectroscopy [6], can quantify blood velocity at high resolution, but are limited to small tissue volumes. Conversely, Particle Image Velocimetry (PIV) methods [2, 7–9] have been used to monitor blood flow

* Corresponding author: e-mail: andreabassi@polimi.it, Phone: +39 02 2399 6010

in zebrafish over large field of views, but do not provide optical sectioning nor reconstruction of blood parameters in three dimensions.

In larger biological samples, Laser Speckle Imaging [10, 11] and Doppler Optical Coherent Tomography (OCT) [12, 13] have been used to measure blood flow, typically in superficial vessels. These two approaches, which are based on coherent light, are not optimally suited to study transparent embryos such as zebrafish due to low scattering of the sample and the detrimental effect on imaging resolution caused by laser speckles.

Here we demonstrate a label free, low cost method able to quantitatively map in 3D, the velocity of blood cells transiting the zebrafish vascular network. Since the actual blood velocity vectors, including their magnitudes and directions, are measured and visualized with single vessel resolution at the whole-organism level, we refer to this method as Optical Vector Field Tomography (OVFT).

2. Methods

2.1 Zebrafish handlings and protocols

All tomography measurements were performed on zebrafish embryos/larvae (*Danio rerio*) belonging to the mutant line *mitfa*$^{w2/w2}$; *roy*$^{a9/a9}$. A mutant transgenic line expressing EGFP in the endothelial cells, *mitfa*$^{w2/w2}$; *roy*$^{a9/a9}$; Tg (*kdrl*:EGFP)^{s843}, was used to obtain Selective Plane Illumination Microscopy images for validation purposes (see Figure 1e).

Zebrafish were ranging from 5 dpf to 15 dpf and were housed in the zebrafish facility of Università degli Studi di Milano, Dipartimento di Bioscienze. They were maintained under standard conditions of temperature (28 °C) and photoperiod (14-hour light/10-hour dark).

In order to study the vascular network, we used a suitable protocol, similar to the ones described for *in vivo* imaging of zebrafish larvae [14, 15]. First, the specimen is anesthetized in 40 mg/l tricaine (Ethyl 3-aminobenzene methansulfonate, Sigma-Aldrich Corporation; Westerfield, 1995). Then, it is transferred in 1.5% low gelling temperature agarose (Sigma, A9414-250G), containing 40 mg/l tricaine as well. The low tricaine concentration anesthetizes the sample without impairing cardiac functions and heart rate, [15] while the relatively high agarose concentration helps in holding it immobilized throughout the measurement. The sample is then mounted inside a FEP tube (Bola, S 1815-07, inner diameter 2 mm, wall thickness 0.5 mm), which is hold vertically, with zebrafish head upwards. The tube is placed inside a square-section glass cuvette filled with water. Since refractive index of FEP tube is 1.338, refractive index matching with water is achieved, thus avoiding optical distortions [14].

All the experimental protocols were reviewed and approved by the Institutional Review Board at the Department of Biosciences of University of Milan. They have been conducted in accordance with National (Italian D.lgs. 116/92) and European laws (2010/63/EU and 86/609/EEC) and regulations controlling experiments on live animals. A project N1/2013 entitled "Zebrafish (*Danio rerio*) as a model system to study cardiovascular system in normal and altered condition" has been submitted as communication to the Ministero del Lavoro, della Salute e delle Politiche Sociali, as requested by National Law. All measurements were performed under tricaine anaesthesia and all efforts were made to minimize animal suffering and the number of animals used.

2.2 Experimental setup and data acquisition

OVFT combines an advanced version of Optical Projection Tomography (OPT) [16], namely Flow-OPT [17], with high speed multi-view acquisition and Particle Image Velocimetry (PIV) analysis. Similarly to X-ray computed tomography, OPT is based on the acquisition of several optical images of a sample taken at different orientations.

The OPT system is schematically depicted in Figure 1a. The white light from an LED is sent through the sample and recollected by telecentric lenses (See Supporting Information). The sample is rotated during the measurement and bright-field images are captured by a camera from several different views. Using a filtered back-projection algorithm, the light absorbing features of the sample can be three-dimensionally reconstructed.

A typical reconstruction of the trunk/tail region (notochord and somites) of a 5 days post fertilization (dpf) zebrafish, depicted in Figure 1b, is shown in grey in Figure 1c. It is superimposed to the vasculature of the specimen (shown in red), which is obtained by Flow-OPT [17]. In this technique, which is based on blood cell motion contrast (See Supporting Information), successive bright-field time-frames are acquired at different orientations of the specimen, typically 400 angular positions. These frames are processed by a motion-analysis algorithm in order to create a 2D vascular map for any angular position around the sample. Successively, these vascular maps are processed mathematically to create a virtual 3D casting of the vasculature. A detail of the vascular network of a 5 dpf zebrafish tail is shown in Figure 1d. For comparison, the same region of the specimen was acquired with Selective Plane Illumination Microscopy (See Supporting Information),

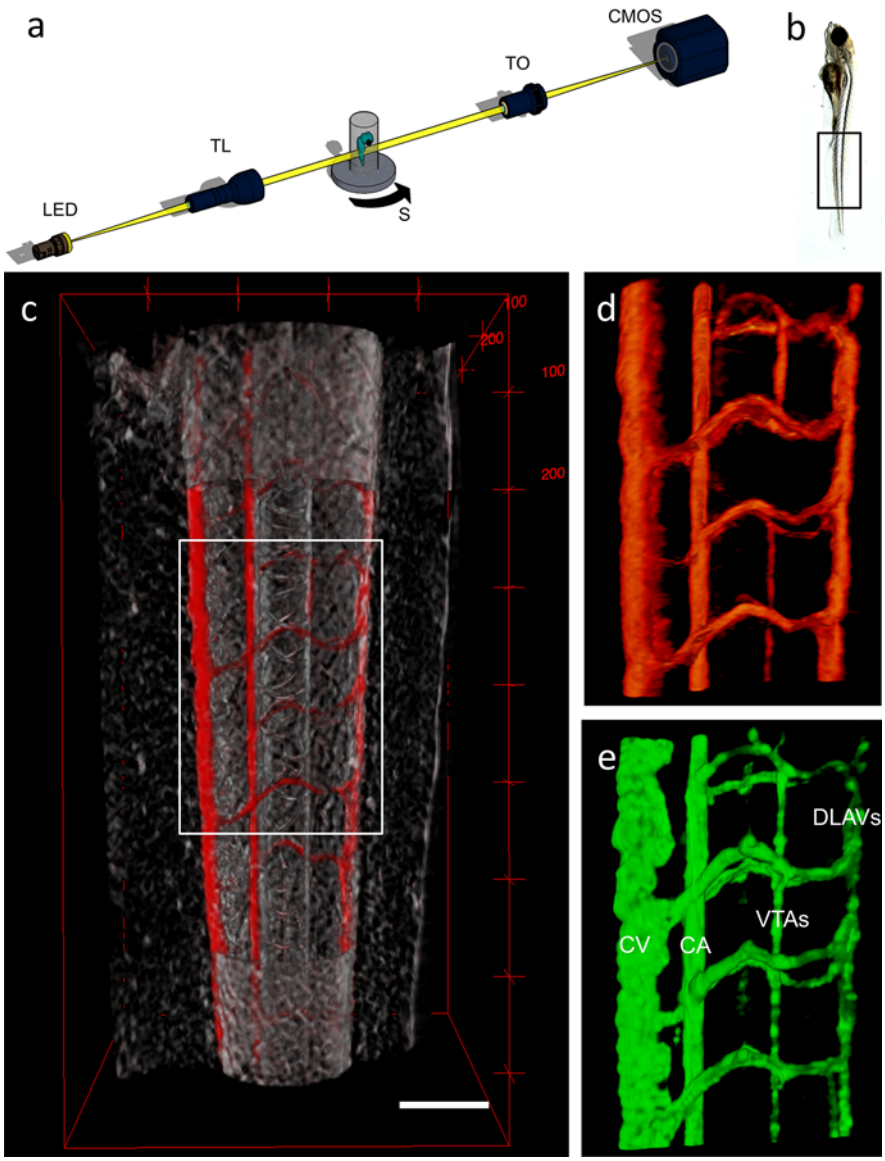

Figure 1 (**a**) Outline of the experimental setup. The light emitted from a white LED is projected on the sample (S) by a telecentric lens (TL). A telecentric objective (TO) creates the bright-field image of the sample on a CMOS camera. The sample is rotated along the vertical axis by a rotation stage (not shown). (**b**) Picture of a 5 dpf zebrafish. The acquisition region is indicated by the black rectangle. (**c**) 3D Reconstruction of the notochord and somites of the zebrafish (grey) obtained with OPT superimposed with the vasculature (red) obtained with Flow-OPT. Scale bar is 100 μm. (**d**–**e**) Close-up of the vasculature obtained with Flow-OPT (**d**) and SPIM (**e**). Flow-OPT visualizes only the patent vessels. Labeled vessels are: Caudal Vein (CV), Caudal Artery (CA), Vertebral Arteries (VTAs) and Dorsal Longitudinal Anastomotic Vessels (DLAVs).

exploiting a specific labeling for blood vessel endothelium. The corresponding 3D reconstruction is shown in Figure 1e.

Flow-OPT offers lower resolution than SPIM (e.g. the Dorsal Longitudinal Anastomotic Vessels are not resolved) but it does not require any fluorescence labeling or transgenic lines, being based only on blood cell motion contrast. Furthermore only patent vessels are visualized and therefore Flow-OPT can potentially be used to examine whether a vessel carries blood cell flow.

2.3 Particle image velocimetry

Figure 1 demonstrates that different levels of morphological information can be acquired with OPT. Functional information can further be obtained with the same instrument, taking advantage of OVFT. In order to recover the 3D velocity vector field, we first developed and characterized a Particle Image Velocimetry (PIV) method, able to obtain bi-dimensional maps of the blood velocity.

By repeating this procedure at four angular positions around the specimen we can then reconstruct the 3D velocity vector field of blood cells (see Results and discussion).

The PIV method is based on the acquisition, at a specific angular position of the sample, of a large number of brightfield images at high frame rate. A typical dataset is made of $M = 100$ successive frames acquired at 80 Hz (see Figure 2a and Supplementary Video 2).

First, the absorption contrast fluctuations are extracted from the dataset by subtracting every bright-

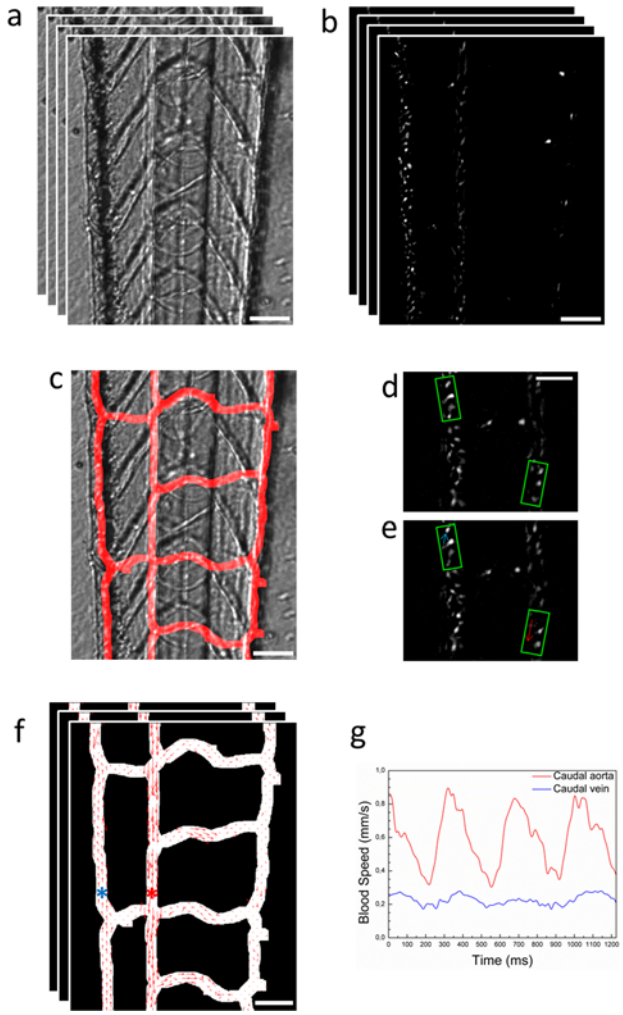

Figure 2 Image processing in PIV analysis. (**a**) Raw brightfield images showing a 5 dpf zebrafish tail. A complete dataset is made up by 100 successive frames. (**b**) Contrast images obtained by subtracting the average intensity image to every brightfield image. They show blood cells as bright spots. (**c**) Segmented image of vessels superimposed in red color on a raw image. (**d**–**e**) Blood cell shift between one frame (**d**) and the successive one (**e**). ROIs are depicted as green rectangles. They are placed on two particular vessels, namely the caudal vein (blue vector, small shift) and the caudal artery (red vector, large shift). (**f**) Planar vector maps obtained with the PIV algorithm. Blue and red asterisks indicate the caudal vein and the caudal artery, respectively. Red arrows show the instantaneous velocity of blood cells. (**g**) Speed versus time profiles for two vectors chosen in correspondence of the asterisks in (**f**). The red curve corresponds to arterial speed profile and shows peaks that relate to the cardiac cycle phases. The blue one corresponds to venous speed profile and shows a more continuous trend, with only large oscillations slightly shifted in phase with respect to the aortic one. Scale bars are: (**a**–**c**, **f**) 50 μm; (**d**–**e**) 30 μm.

field image $I(x, y, t)$ from the time-average intensity image $\langle I(x,y,t)\rangle_t$:

$$\delta I(x,y,t) = \langle I(x,y,t)\rangle_t - I(x,y,t) \quad (1)$$

This calculation results in M contrast frames, which indicate blood cells positions, as shown in Figure 2b and Supplementary Video 3. The more a cell attenuates light during its motion, the brighter its contrast image is. This is an important pre-processing step, since it increases the signal-to-noise ratio and it eliminates the contribution of immobile structures, which could produce artifacts when the PIV algorithm is operated.

In order to perform an efficient PIV analysis, it is necessary to extract the vessel positions on the contrast images. The use of this a priori information reduces the time required for processing, while on the other side it eliminates false velocity measurements due to background noise.

Vessel positions are obtained by applying Eq. (1) to the set of raw images. The resulting images are then summed together and segmented in order to create a binary mask, as shown in Figure 2c.

The binary mask is used to create several rectangular Regions Of Interests (ROIs) over the vessels, on which the PIV analysis is performed, as depicted in Figure 2d–e. The widths of the rectangles (aligned with the vessels direction) are assumed of $w = 50$ pixels, while their heights h are adapted to the vessel cross-section. In this way, regions outside the vessels are not considered. The number of ROIs is chosen in order to have 50% overlap between each ROI and its neighboring ones. The width w of the major axis can be optimized on a case-by-case basis in order to set the theoretical maximum speed detectable well above the one that is expected from the sample under study.

The particle displacement inside a ROI is quantified by a PIV analysis, which consists in a spatio-temporal cross-correlation (C_k), between each k-th frame and the successive one, of ROI intensity (I_{ROI}):

$$C_k = \int\int I^*_{\mathrm{ROI},k+1}(\xi,\eta)\cdot I_{\mathrm{ROI},k}(x+\xi, y+\eta)\,\mathrm{d}\xi\,\mathrm{d}\eta \quad (2)$$

Where I^* denotes the complex conjugate of I, ξ and η are spatial lag variables, which correspond to pixel shifts of the intensity in x and y directions, respectively. Correlation is computed with a custom written software, based on the OpenPIV toolbox (http://www.openpiv.net/) [18].

The code calculates the cross-correlation C_k thanks to the convolution theorem as:

$$C_k = \mathscr{F}^{-1}\{\mathscr{F}[I^*_{\mathrm{ROI},k+1}(-x,-y)]\cdot\mathscr{F}[I_{\mathrm{ROI},k}(x,y)]\} \quad (3)$$

where $\mathscr{F}$ denotes the Fourier transform. Note that it is necessary to compute $I^*_{\mathrm{ROI},\,k+1}$ in $(-x, -y)$, i.e. to mirror the function with respect to the origin, for retrieving the cross-correlation, instead of convolution.

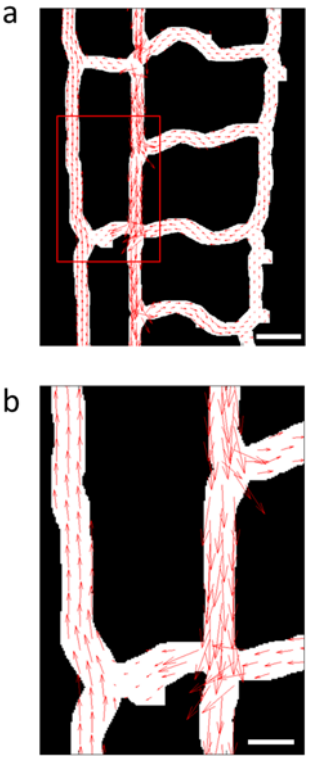

Figure 3 Mean blood velocity vector map. (**a**) Mean velocity map resulting from the average of all planar velocity maps over 1.25 ms (about four cardiac cycles). (**b**) Close-up of the highlighted region in (**a**). Scale bars are: (**a**) 50 μm; (**b**) 20 μm.

We calculated that, with a frame rate of 80 Hz and a pixel size of 0.65 μm/pixel, the method has a resolution of about 0.025 mm/s, assuming minimum detectable displacements of half a pixel. However, this is a conservative estimate, since a Gaussian curve-fitting method is used in the algorithm to achieve subpixel resolution of about 1/10 [19].

Starting from M frames, the algorithm calculates M-1 planar velocity maps (Figure 2f), since the velocity is calculated between pairs of images. Velocity maps show the vectors associated to the entire set of ROIs over the image. The direction of each vector indicates the mean spatial flow direction in each ROI, while the magnitude corresponds to the local blood speed, calculated as: $v = \Delta s \; d \; f$, where Δs is the displacement detected by the cross-correlation analysis on each ROI pairs in pixels, d is the image pixel size in millimeters and f is the acquisition frame rate. From the complete sequence of velocity maps (see Supplementary Video 4), it is possible to extract the profile of blood speed as a function of time for chosen vectors of interest. This can be used to monitor how the blood cells speed evolves in time inside specific vessels, as shown in Figure 2g.

Alternatively, the (M-1) planar velocity maps can be processed to obtain the blood velocity averaged over one or more heart cycles. We chose to calculate the root mean square blood velocity in time, which gives an overall view of blood dynamics in the vascular network. In this case, for every ROI, the direction $\grave{e}$ of the mean vector is calculated as:

$$\theta = \arctan\left(\frac{\sum_{i=1}^{M-1} v_{y,i}}{\sum_{i=1}^{M-1} v_{x,i}}\right) \tag{4}$$

where $v_{y,i}$ and $v_{x,i}$ are the vertical y-component and horizontal x-component of ROI velocity vector, respectively, for the i-th velocity map. The magnitude V of the mean vector, instead, is computed as the root mean square velocity:

$$V = \sqrt{\frac{\sum_{i=1}^{M-1} (v_{x,i}^2 + v_{y,i}^2)}{M-1}} \tag{5}$$

The mean vector map obtained by averaging over four cardiac cycles can be seen in Figure 3a–b.

3. Results and discussion

In order to perform Optical Vector Field Tomography, images are acquired at high frame rate for four distinct views, (namely 0°, 90°, 180° and 270°) and the PIV algorithm is repeated, yielding four planar mean velocity maps, averaged over a few heart cycles.

Then, the four velocity maps are projected on the virtual vasculature of the sample, which is divided in four volumes, as depicted in Figure 4a. In particular, two velocity maps, orthogonal to each other, are associated to each of the four volumes. The vector field tomography algorithm scans the voxels contained in the first transverse slice of the virtual vascular network. Once a vessel is encountered, the voxel position is projected onto the two planar vector maps associated with the voxel quadrant. If two non-zero vectors are found in the bi-dimensional maps, they are combined to yield the actual vector in the 3D space.

Consider two planar vector maps out of four. Supposing that z is the vertical axis, a vector in the first map ($v_{1,xz}$) represents the projection of the actual vector in the 3D space over the $x-z$ plane, while the corresponding one on the other planar map ($v_{2,yz}$) is the projection over the $y-z$ plane. Thus, the following two vectors are associated to a voxel of the vascular network:

$$\boldsymbol{v}_{1,xz} : \begin{cases} v_{1,x} = V \cos\left(\overset{/\!\!\backslash}{xV}\right) \\ v_{1,z} = V \cos\left(\overset{/\!\!\backslash}{zV}\right) \end{cases}$$

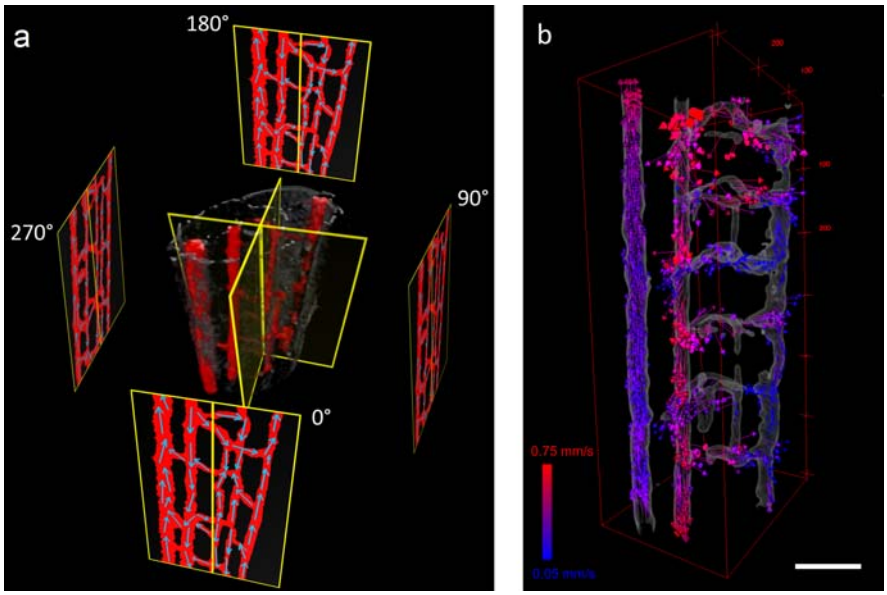

Figure 4 Vector field tomography principle. (**a**) The projections of blood velocity are measured from four orthogonal views and the obtained values are back-projected on the vascular network. (**b**) Reconstructed 3D blood velocity vector field over a 600 μm long trunk portion of a 5 dpf zebrafish. Vectors are color encoded (blue to red) and their lengths are proportional to the calculated speeds. Scale bar is 100 μm.

$$\boldsymbol{v}_{2,yz}: \begin{cases} v_{2,y} = V\cos\left(\overset{/\!\backslash}{yV}\right) \\ v_{2,z} = V\cos\left(\overset{/\!\backslash}{zV}\right) \end{cases}$$

where $\boldsymbol{V}$ represents the actual vector in 3D space and $\cos\left(\overset{/\!\backslash}{xV}\right)$, $\cos\left(\overset{/\!\backslash}{yV}\right)$, $\cos\left(\overset{/\!\backslash}{zV}\right)$ are the direction cosines of $\boldsymbol{V}$ in a x, y and z reference system. In order to reconstruct the vector $\boldsymbol{V}$, the two vector components $\boldsymbol{v}_{1,xz}$ and $\boldsymbol{v}_{2,yz}$ are combined in the following way:

$$\boldsymbol{V}: \begin{cases} V_x = V\cos\left(\overset{/\!\backslash}{xV}\right) = v_{1,x} \\ V_y = V\cos\left(\overset{/\!\backslash}{yV}\right) = v_{2,y} \\ V_z = V\cos\left(\overset{/\!\backslash}{zV}\right) = \dfrac{v_{1,z} + v_{2,z}}{2} \end{cases} \tag{8}$$

In particular, the magnitudes of the vertical components are averaged, since they should be exactly the same, while the two horizontal components are taken as they are from the two planar maps respectively, since they are orthogonal to each other and aligned with the x and y axes. This algorithm is then repeated for all the transverse slices of the sample, creating a 3D velocity vector field of the zebrafish vascular network. Finally, they are back-projected onto the segmented 3D virtual structure of the vascular network, previously reconstructed with Flow-OPT.

It is worth noting that it is important to choose the starting 0° position carefully: in the segmented contrast images of the 4 angular positions, the vascular network should be displayed with as little overlapping between vessels as possible. Regarding zebrafish larvae, for example, one wants to avoid the dorsal and the ventral views, since the great majority of vessels is aligned along a very narrow region around the spine. As a result, the best starting angular position is 45° apart from the dorsal view (Figure 4a).

The OVFT results obtained on a 600 μm portion of a 5 dpf zebrafish tail are shown in 3D in Figure 4b, superimposed to the vascular network. The flow speed is color encoded and proportional to the visualized vector length. Except for high flux regions, such as the caudal artery that presents a high degree of turbulence, the majority of vectors is aligned with the vessel direction, even if the algorithm does not force any vector to be parallel to vessels, but only to originate from them.

The results from a smaller portion of the 5 dpf zebrafish tail (about 250 μm long), in correspondence to the anal fin, are shown in Figure 5a, b. The vascular network present in the chosen tail region is sketched for clarity in Figure 5c. It can be noted that all the vessels allow blood cells to circulate, with flow direction and magnitudes coherent with the expected ones. We measured a speed of 0.71 ± 0.13 mm/s ($n = 6$ samples) in the caudal artery. The mean velocity in the caudal vein, instead, is of 0.20 ± 0.09 mm/s ($n = 6$), in agreement with previous reports [7, 8, 20]. The best way to visualize the distribution of speed values inside different vessels is achieved by removing the vectors and by color encoding the vessels as a function of speed, as depicted in Figure 5d. Very low speeds, such as those present in the vertebral arteries, fall below the temporal resolution of the system and slower frame rate acquisitions would be required to detect cell motion in those compartments.

Vector field tomography reconstructions of zebrafish at two developmental stage, 6 dpf and 15 dpf, are shown in Figure 5e, f. During embryos growth,

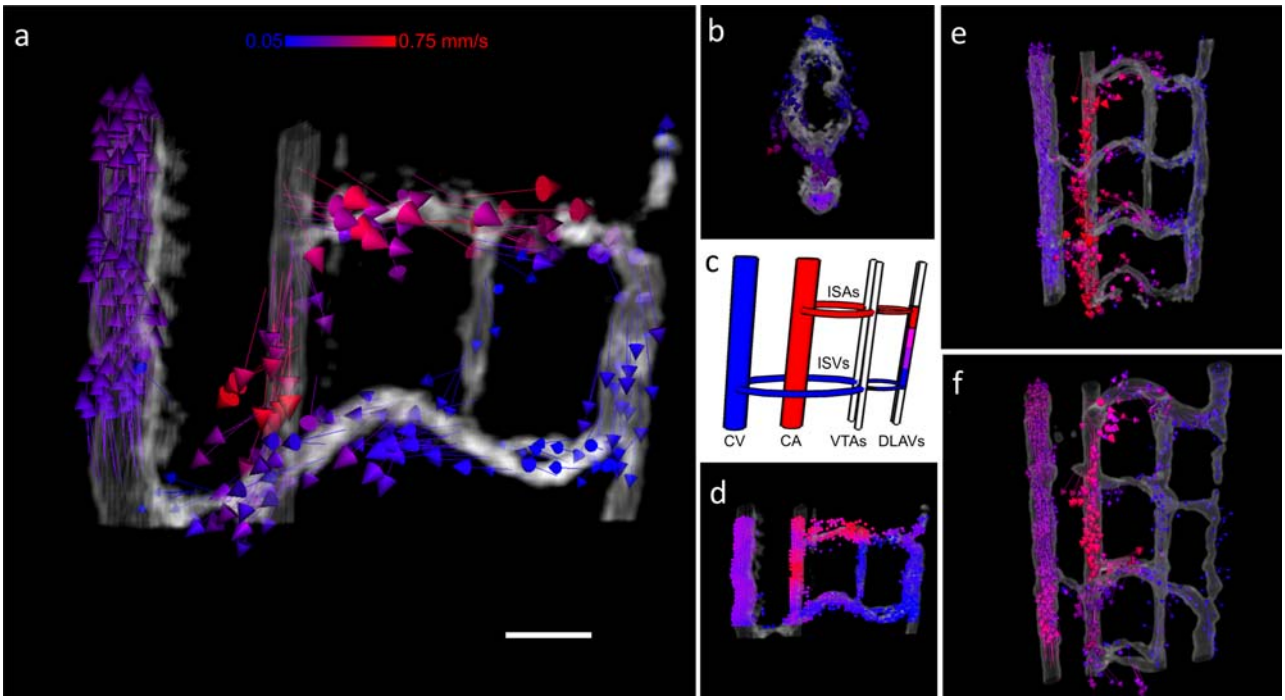

Figure 5 (**a**) Velocity vector field of a region of the 5 dpf zebrafish tail that includes Inter-Segmental Arteries (ISAs) and Inter-Segmental Veins (ISVs). The 3D model is oriented to show the zebrafish lateral view (dorsal part is on the right side). Scale bar is 50 μm. (**b**) Transverse view of the 3D model, showing the same region from the bottom (dorsal part is on top). (**c**) Schematic of the region showing: Caudal Vein (CV), Caudal Artery (CA), Vertebral Arteries (VTAs), Dorsal Longitudinal Anastomotic Vessels (DLAVs). Arterial vessels are indicated in red, venous vessels in blue. Newly formed vessels are indicated in white. (**d**) Vessels, belonging to the same region shown in (**a**), are color encoded as a function of speed. (**e**) Velocity vector field of a 6 dpf zebrafish. (**f**) Velocity vector field of a 15 dpf zebrafish.

we measured a decrease in caudal artery blood speed (-15%, $n = 3$ samples) and an increase in caudal vein flow ($+7\%$, $n = 3$ samples), together with a substantial improvement in vertebral artery circulation.

When the specimen is about 20 dpf, the large scattering of the sample and the difficulties in immobilizing the larvae limit the applicability of OVFT.

4. Conclusion

In this paper we present a new quantitative approach to visualize in 3D the vector field associated to blood velocity in small transparent organisms, without the use of any staining or fluorescent probe.

Our technique, coupled with minimally invasive mounting protocols [15], represents a novel tool for the study of zebrafish development, since the specimen could be analyzed repeatedly over several days. It is worth noting that tissue photo-toxicity is avoided, thanks to the use of only brightfield illumination.

The technique is extremely low cost and it could be integrated in a variety of fluorescence-based microscopes. In particular OVFT shares similar sample holders and detection optics with SPIM. A combined instrument could not only be used to screen blood flow within the vascular network, but could also represent a new tool able to investigate the interplay between hemodynamic parameters and genetically programmed patterning cues.

In principle, two angular positions were sufficient to reconstruct the 3D velocity vector field, but the use of only two views would cause shielding artefacts. Indeed, if two vessels were one in front of the other in the depth of field of the objective, the blood cell motion in the front vessel would shield the motion present in the rear one. Instead, by acquiring four views, we can virtually divide the sample in four volumes treated indipendently, thus reducing shielding artifacts. A larger number of views could be potentially used to further improve this procedure, at the expense of an increased measurement time.

The present technique could be designed, in future, for synchronous acquisitions by 4 distinct cameras: four views could be acquired in parallel, allowing one to perform PIV analysis on simultaneous data and to determine the instantaneous velocity vector field, rather than the mean one.

Acknowledgements This work was partially supported by Cariplo Foundation under Grant N. 2009–2626. E.A.F. acknowledges support from Adriano Buzzati-Traverso Foundation.

Author biographies Please see Supporting Information online.

References

[1] S. Isogai, N. D. Lawson, S. Torrealday, M. Horiguchi, and B. M. Weinstein, Development **130**(21), 5281–5290 (2003).
[2] J. R. Hove, R. W. Köster, A. S. Forouhar, G. Acevedo-Bolton, S. E. Fraser, and M. Gharib, Nature **421**, 172–177 (2003).
[3] N. D. Lawson and B. M. Weinstein, Dev. Biol **248**(2), 307–318 (2002).
[4] J. Huisken, J. Swoger, F. Del Bene, J. Wittbrodt, and E. H. K. Stelzer, Science **305**, 1007–1009 (2004).
[5] F. O. Fahrbach, F. F. Voigt, B. Schmid, F. Helmchen, and J. Huisken, Optics Express, **21**(18), 21010–21026 (2013).
[6] X. Pan, H. Yu, X. Shi, V. Korzh, and T. Wohland, J. Biomed. Opt. **12**(1), 014034 (2007).
[7] C. Y. Chen, M. J. Patrick, P. Corti, W. Kowalski, B. L. Roman, and K. Pekkan, Biorheology **48**, 305–321 (2011).
[8] S. C. Watkins, S. Maniar, M. Mosher, B. L. Roman, M. Tsang, and C. M. St Croix, PLoS ONE **7**(8), e44018 (2012).
[9] R. A. Jamison, A. Fouras, and R. Bryson-Richardson, J. Biomed. Opt. **17**(3), 036007 (2012).
[10] A. K. Dunn, H. Bolay, M. A. Moskowits, and D. A. Boas, J. Cereb. Blood Flow Metab. **21**, 195–201 (2001).
[11] B. Choi, N. M. Kang, and J. S. Nelson, Microvasc. Res. **68**(2), 143–146 (2004).
[12] R. K. Wang, S. L. Jacques, Z. Ma, S. Hurst, S. R. Hanson, and A. Gruber, Opt. Express **15**(7), 4083–4097 (2007).
[13] L. An and R. K. Wang Opt. Lett. **36**(6), 831–833 (2011).
[14] A. M. Petzold, V. M. Bedell, N. J. Boczek, J. J. Essner, D. Balciunas, K. J. Clark, and S. C. Ekker, Zebrafish **7**, 149–154 (2010).
[15] A. Kaufmann, M. Mickoleit, M. Weber, and J. Huisken, Development **139**, 3242–3247 (2012).
[16] J. Sharpe, U. Ahlgren, P. Perry, B. Hill, A. Ross, J. Hecksher-Sorensen, R. Baldock, and D. Davidson, Science. **296**, 541–545 (2002).
[17] A. Bassi, L. Fieramonti, C. D'Andrea, M. Mione, and G. Valentini, J. Biomed. Opt. **16**, 100502 (2011).
[18] Z. J. Taylor, R. Gurka, G. A. Kopp, and A. Liberzon, IEEE T. Instrum. Meas. **59**, 3262–3269 (2010).
[19] H. Huang, D. Dabiri, and M. Gharib, Meas Sci. Technol. **8**, 1427–1440 (1997).
[20] R. Kopp, T. Schwerte, M. Egg, A. M. Sandbichler, B. Egger, and B. Pelster, Physiol. Genomics **42A**, 8–23 (2010).